frontiers

SUPPLEMENTARY INFORMATION

on

Optimizing control strategies for urine nitrification: Narrow pH control band enhances process stability and reduces nitrous oxide emissions

Contents

1 Main reactor set-up

The 12-L reactor consisted of a continuous-flow stirred-tank reactor (CSTR) without sludge retention (hydraulic retention time = solid retention time), as shown in **Figure S1**. The reactor was fed from the middle with a peristaltic pump (PD-5001, Heidolph) using pumping tubes with a wall thickness of 1.6 mm and an inner diameter of 1.6 mm. For the effluent, the reactor had an overflow on the top. The reactor was equipped with an overhead stirrer (RZR 2020 Overhead Stirrer, Heidolph), a pressure gauge (Cerabar T PMC131, Endress+Hauser), a pH sensor (Orbisint CPS11D, Endress+Hauser), and a DO sensor (Oxymax COS61D, Endress+Hauser). The temperature was also measured with the pH sensor (Orbisint CPS11D, Endress+Hauser). The temperature was controlled via a water heat jacket (FN25, Julabo).

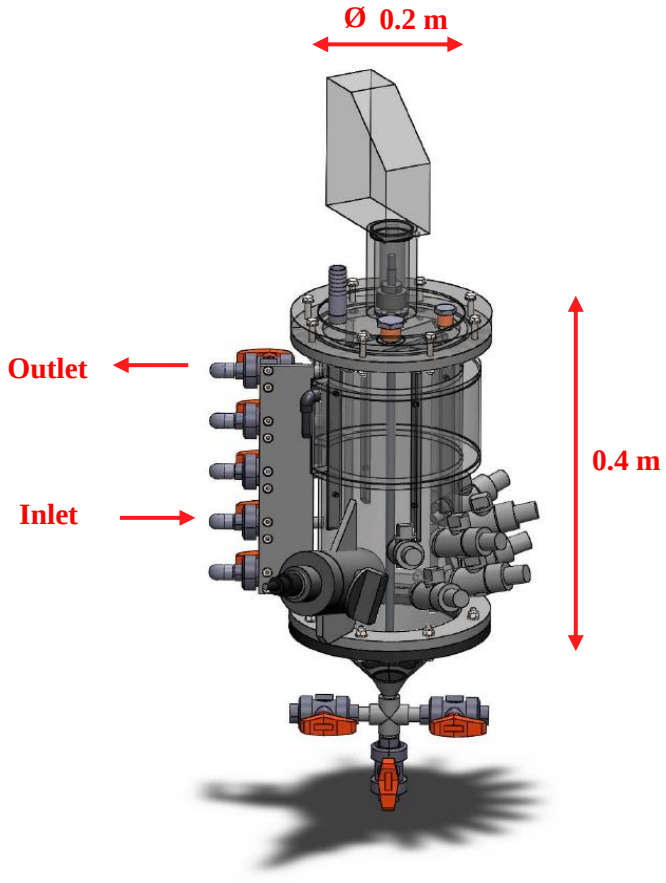

Figure S1: Dimension of the 12-L lab scale reactors (picture © Adriano Joss, Eawag).

2 Model description

The process failures were simulated using the SUMO19 wastewater treatment software developed by Dynamita (France). The Sumo2 model was modified to include the switching functions and kinetic parameters shown in Table 3. The model consisted of an aerated CSTR for nitrification and a two-point controller with pH as the controlled variable and influent as the manipulated variable (**Figure S2**).

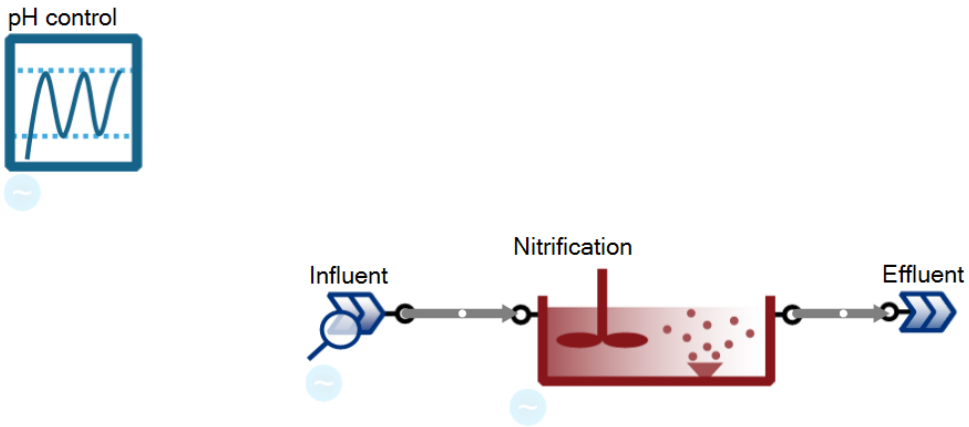

Figure S2: Sumo model process configuration for the main reactor. The nitrification was integrated as 2-L CSTR. The pH control was used to control the pH with the influent within an upper and lower limit.

The focus of the model was on nitrification, thus, no heterotrophic bacteria were included. The influent parameters are presented in **Table S1**. The concentrations correspond to the average influent concentrations for the 12-L reactors. The initial reactor concentrations are shown in **Table S2**. A maximum growth rate of 1.21 d^{-1} and a decay rate of 0.2 d^{-1} were used for the AOB, and a maximum growth rate of 1.02 d^{-1} and a decay rate of 0.17 d^{-1} were used for the NOB (Jubany et al., 2008).

Table S1: Influent composition in the Sumo model.

Variable	Unit	Concentration
Total ammoniacal-nitrogen	[mg-N L^{-1}]	3210
Total inorganic carbon	[mg-C L^{-1}]	1620
Total phosphate	[mg-P L^{-1}]	128
Potassium	[mg L^{-1}]	1082
Sodium	[mg L^{-1}]	1257
Total sulfate	[mg-S L^{-1}]	135
Chloride	[mg L^{-1}]	2300

Table S2: Initial concentration of the nitrification in the Sumo model.

Variable	Unit	Concentration
Total ammoniacal-nitrogen	[mg-N L^{-1}]	1605
Nitrate-nitrogen	[mg-N L^{-1}]	1605
Total inorganic carbon	[mg-C L^{-1}]	0
Total phosphate	[mg-P L^{-1}]	128
Potassium	[mg L^{-1}]	1082
Sodium	[mg L^{-1}]	1257
Total sulfate	[mg-S L^{-1}]	135
Chloride	[mg L^{-1}]	2300
AOB	[mg-COD L^{-1}]	100
NOB	[mg-COD L^{-1}]	100

To simulate the process failures used for the robustness tests, the model was always run for 15 days to reach a steady state and then changed accordingly (**Table S3**).

Table S3: Variable modified in the SUMO model before and after day 15.

Modified variable	Disturbance	Possible failure
Temperature	25°C → 30°C	Nitrite accumulation
pH set-points	6.2/6.25 → 6.4/6.45 and 6.0/6.5 → 6.2/6.7	Nitrite accumulation
Dissolved oxygen concentration	7 mg L^{-1} → 1.5 mg L^{-1}	Nitrite accumulation

3 Acid-base equilibrium for ammonium and ammonia

The acid-base equilibrium for ammonium and ammonia is shown in **Equation S1**.

$$NH_4^+ \rightleftharpoons NH_3 + H^+ \qquad (S1)$$

Equilibrium concentrations were calculated according to **Equations S2**, **S3** (Crittenden et al., 2012), **S4** (Anthonisen et al., 1976), **S5** (Lewis and Randall, 1921), and **S6** (Davies, 1967) following the description in Crittenden et al. (2012).

$$[TAN] = [NH_3] + [NH_4^+] \qquad (S2)$$

$$K_a(T) = \frac{[NH_3] \times [H^+] \times f_{mono}}{[NH_4^+] \times f_{mono}} = \frac{[NH_3] \times 10^{-pH}}{[NH_4^+] \times f_{mono}} \qquad (S3)$$

$$K_a(T) = e^{\frac{-6344}{T}} \qquad (S4)$$

$$I = \frac{1}{2} \times \sum_i [C_i] \times Z_i^2 \qquad (S5)$$

$$\log_{10} f_{mono} = -A * \left(\frac{I^{0.5}}{1 + I^{0.5}} - 0.3 * I \right) \qquad (S6)$$

All variables are shown in **Table S4**.

Table S4: All variables used in the equations S1 to S6.

Variable	Name	Unit
[TAN]	Total ammonia nitrogen	[mol L^{-1}]
[NH_3]	Ammonia concentration	[mol L^{-1}]
[NH_4^+]	Ammonium concentration	[mol L^{-1}]
[H^+]	Proton concentration	[mol L^{-1}]
K_a	Dissociation constant, pK_a=9.25 @25°C	[mol L^{-1}]
f_{mono}	Activity coefficient for monovalent ions	[-]
T	Absolute temperature, 298 K @25°C	[K]
I	Ionic strength	[mol L^{-1}]
[C_i]	Concentration of ionic specie i	[mol L^{-1}]
Z_i	Charge of ionic specie i	[-]
A	0.51 at 25°C (Stumm and Morgan, 1996)	[-]

For the calculation of the ionic strength, the main ionic species in nitrified urine were considered: K^+, Cl^-, Na^+, NH_4^+, NO_3^-, NO_2^-, $H_2PO_4^-$, and SO_4^{2-}. The ionic strength calculated for this publication was between 0.05 M to 0.2 M. For ionic strength below 0.1 M, the Davies equations (**Equation S6**) typically is in error by 1.5%, and for ionic strength between 0.1 M to 0.5 M an error of 5% to 10% can be expected (Levine, 1988).

4 Acid-base equilibrium for nitrous acid and nitrite

The acid-base equilibrium for nitrous acid and ammonia is shown in **Equation S7**.

$$HNO_2 \leftrightarrow NO_2^- + H^+ \qquad (S7)$$

Equilibrium concentrations were calculated according to **Equations S8**, **S9** (Crittenden et al., 2012), **S10** (Anthonisen et al., 1976), **S11** (Lewis and Randall, 1921), and **S12** (Davies, 1967), following the description in Crittenden et al. (2012).

$$[TNN] = [HNO_2] + [NO_2^-] \qquad (S8)$$

$$K_a(T) = \frac{[NO_2^-] \times f_{mono} \times [H^+] \times f_{mono}}{[HNO_2]} = \frac{[NO_2^-] \times f_{mono} \times 10^{-pH}}{[HNO_2]} \qquad (S9)$$

$$K_a(T) = e^{\frac{-2300}{T}} \qquad (S10)$$

$$I = \frac{1}{2} \times \sum_i [C_i] \times Z_i^2 \qquad (S11)$$

$$\log_{10} f_{mono} = -A * \left(\frac{I^{0.5}}{1 + I^{0.5}} - 0.3 * I \right) \qquad (S12)$$

All variables are shown in **Table S5**.

Table S5: All variables used in equations S7 to S12.

Variable	Name	Unit
[TNN]	Total nitrite nitrogen	[mol L^{-1}]
[HNO_2]	Nitrous acid concentration	[mol L^{-1}]
[NO_2^-]	Nitrite concentration	[mol L^{-1}]
[H^+]	Proton concentration	[mol L^{-1}]
K_a	Dissociation constant, pK_a=3.35 @25°C	[mol L^{-1}]
f_{mono}	Activity coefficient for monovalent ions	[-]
T	Absolute temperature, 298 K @25°C	[K]
I	Ionic strength	[mol L^{-1}]
[C_i]	Concentration of ionic specie i	[mol L^{-1}]
Z_i	Charge of ionic specie i	[-]
A	0.51 at 25°C (Stumm and Morgan, 1996)	[-]

For the calculation of the ionic strength, the main ionic species in nitrified urine were considered: K^+, Cl^-, Na^+, NH_4^+, NO_3^-, NO_2^-, $H_2PO_4^-$, and SO_4^{2-}. The ionic strength calculated for this publication was between 0.05 M to 0.2 M. For ionic strength below 0.1 M, the Davies equations (**Equation S12**) typically is in error by 1.5%, and for ionic strength between 0.1 M to 0.5 M an error of 5% to 10% can be expected (Levine, 1988).

5 Short-term fluctuations

While short-term fluctuations in pH caused variations in TNN, TAN, and nitrate concentrations were constant during a pH cycle for both operating strategies. (**Figure S3**). Faust et al. (2023) reported that the amount of ammonia being oxidized does not change between pH 6 and 7, as the system is poorly buffered in this pH range. While slightly less nitrite is oxidized to nitrate at pH 6.5, changes in nitrate concentration are within the measurement uncertainty.

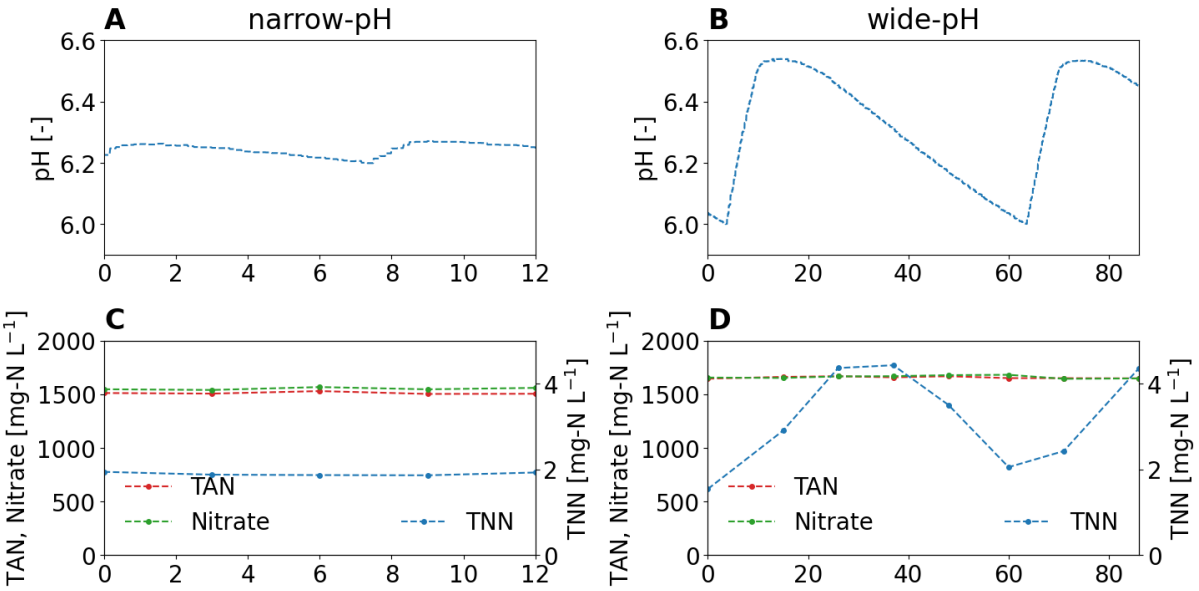

Figure S3: Influence of short-term pH fluctuations on nitrogen concentrations. (A, C) The narrow-pH reactor was operated with pH set-points of 6.2 and 6.25. (B, D) The wide-pH reactor was operated with pH set-points of 6.0 and 6.5.

6 Reactor performance

Figures S4, **S5**, **S6**, **S7,** and **S8** display various aspects of the system's performance. **Figure S4** shows the specific nitrification rate and the solid retention time, providing insights into the system's efficiency. **Figure S5** illustrates the TAN and nitrate concentration. **Figure S6** presents the TSS, VSS, total COD, and soluble COD. In **Figure S7**, the phosphate, potassium, sulfate, sodium, calcium, and conductivity concentrations are displayed. Finally, **Figure S8** shows the temperature, pH and dissolved oxygen concentration in both reactors.

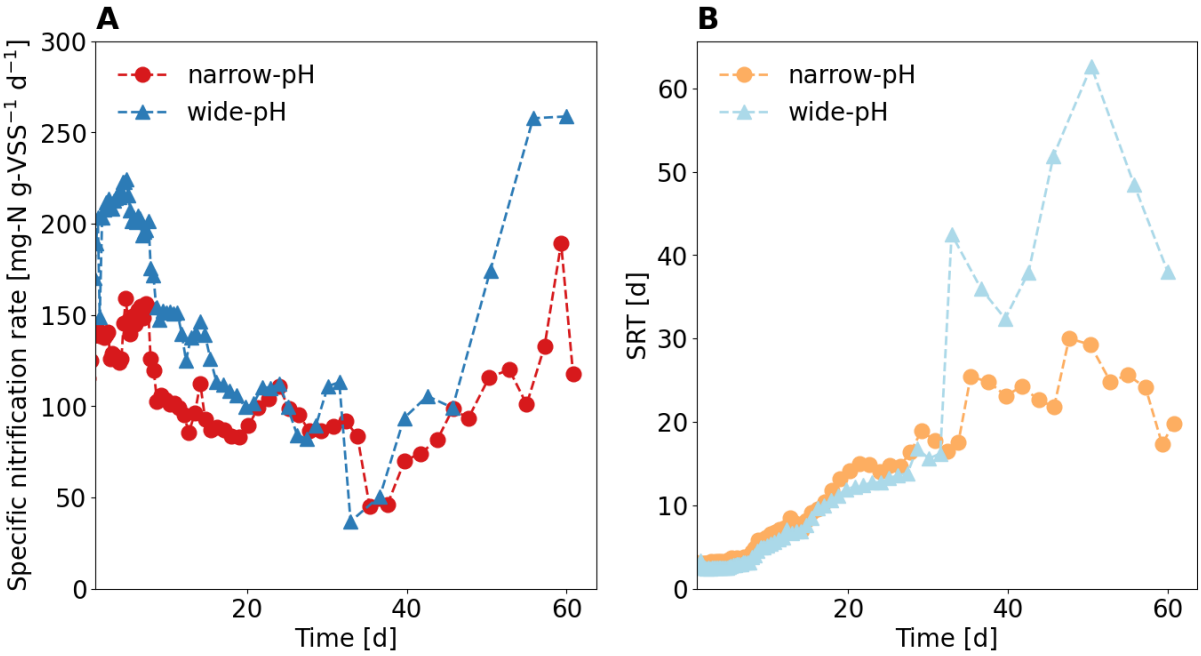

Figure S4: (A) Specific nitrification rates were higher for the wide-pH reactor at 140 ± 60 mg-N g-VSS^{-1} d^{-1} than for the narrow-pH reactor at 100 ± 30 mg-N g-VSS^{-1} d^{-1}. (B) The solid retention time (SRT) increased strongly in both reactors.

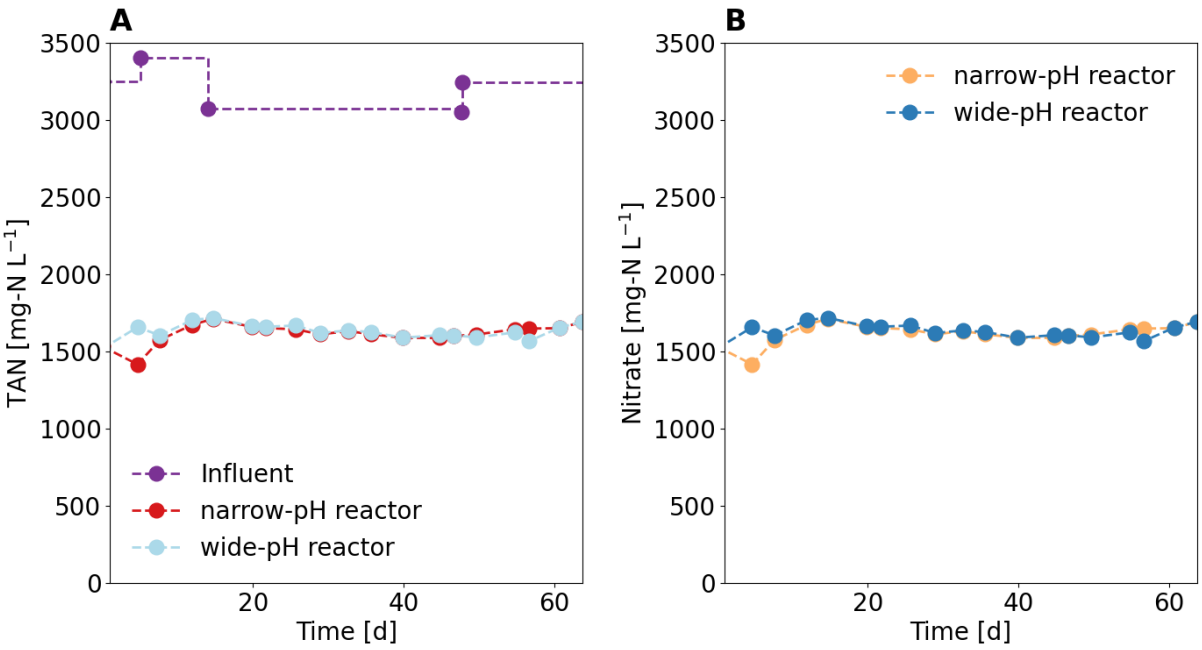

Figure S5: (A) TAN concentrations in the wide- and narrow-pH reactor, and the influent (B) Nitrate concentration in the wide- and narrow-pH reactor.

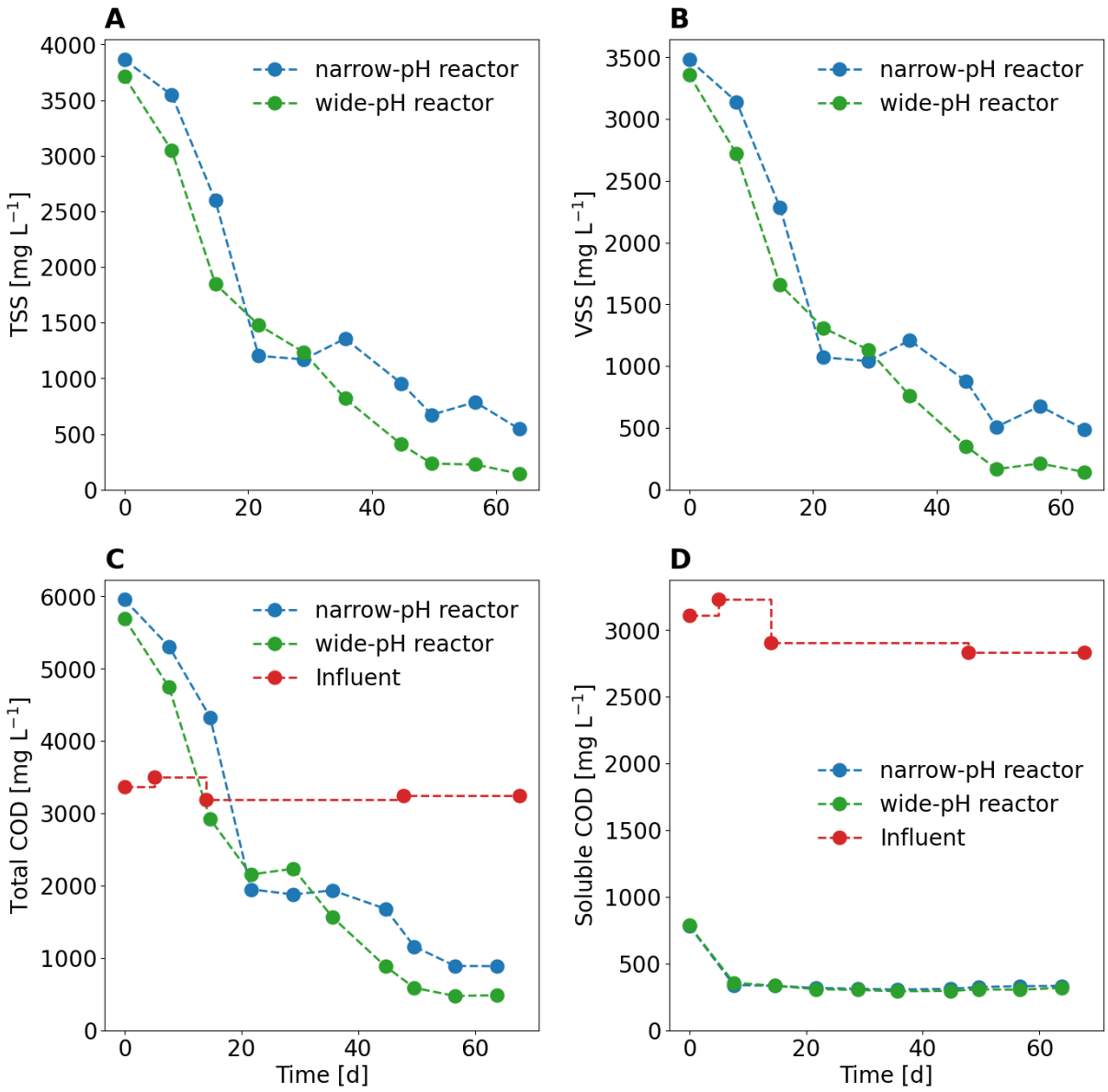

Figure S6: (A) TSS concentrations in the wide- and narrow-pH reactor (B) VSS concentrations in the wide and narrow-pH reactor (C) Total COD concentrations in the wide- and narrow-pH reactor, and the influent (D) Soluble COD concentrations in the wide- and narrow-pH reactor, and the influent.

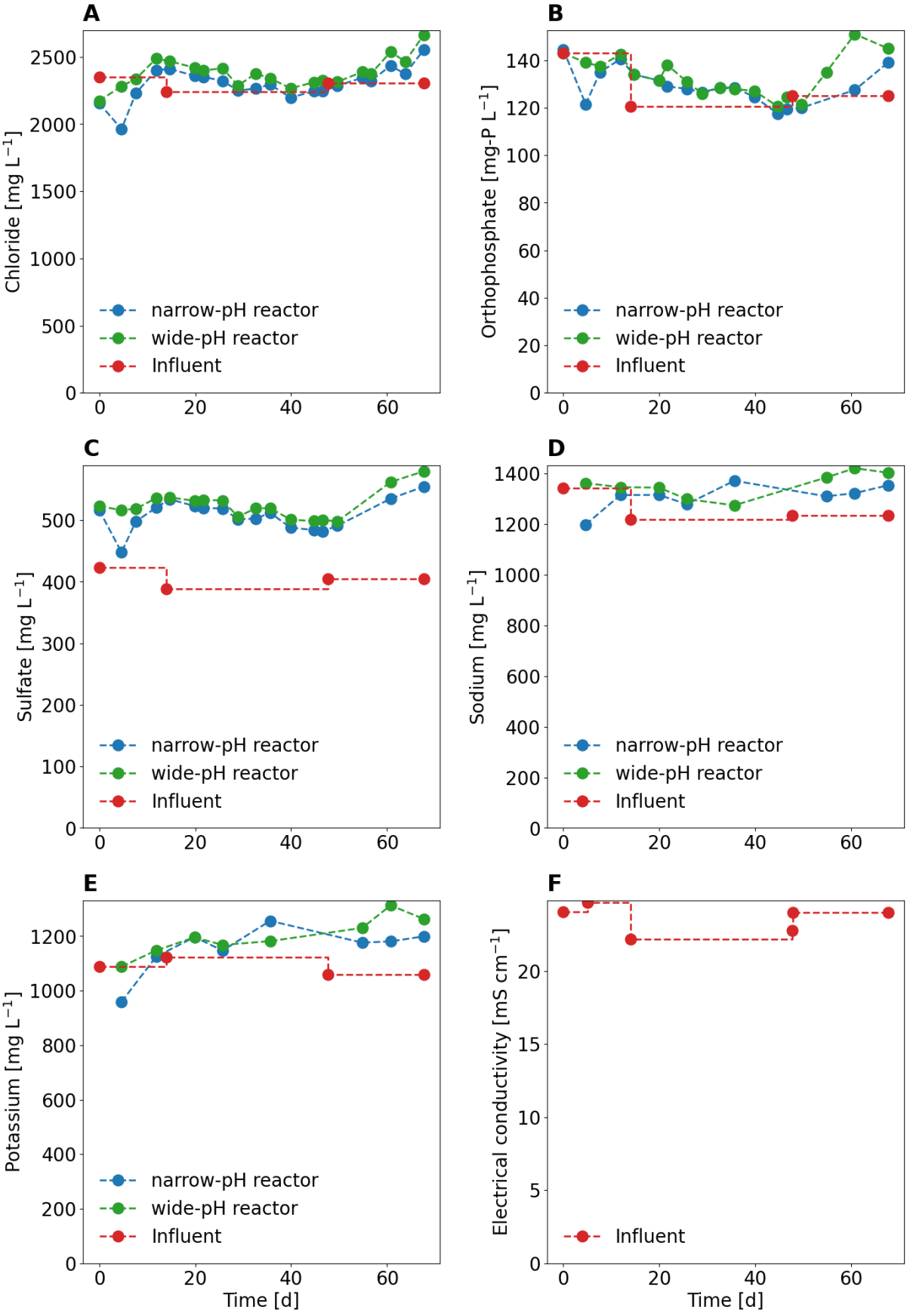

Figure S7: Concentrations of ions and conductivity in the wide- and narrow-pH reactor and the influent.

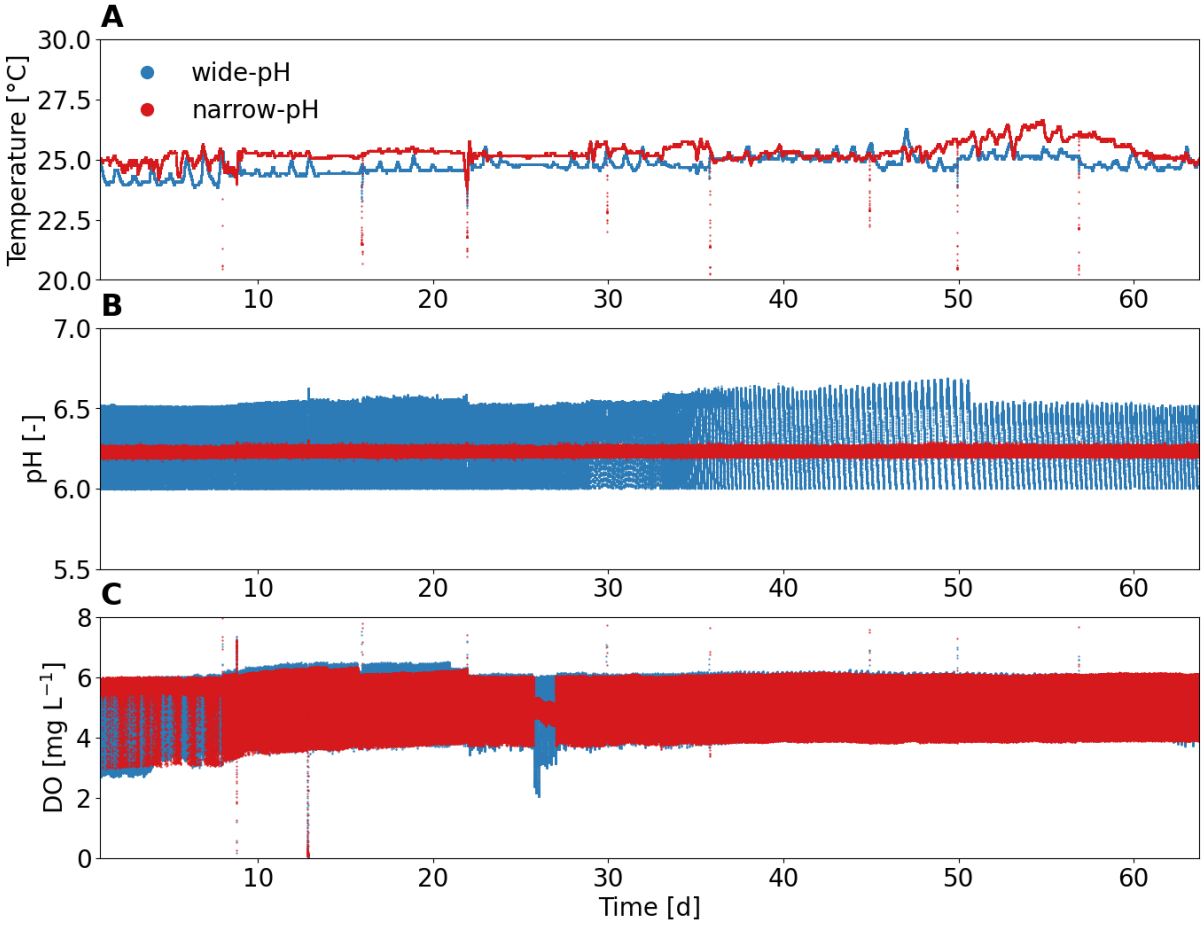

Figure S8: (A) The temperature was controlled at approximately 25°C. (B) The pH was controlled either between either 6.20 to 6.25 (narrow-pH) or 6.00 to 6.50 (wide-pH). (C) The dissolved oxygen (DO) concentration was controlled between 4 and 6 mg L^{-1}.

7 N_2O emissions

The N_2O emission in the wide-pH reactor was, on average, 0.5% of the nitrogen load and, therefore, significantly ($p<0.05$) greater than the N_2O emission factor of 0.25% for the narrow-pH reactor (**Figure S9**).

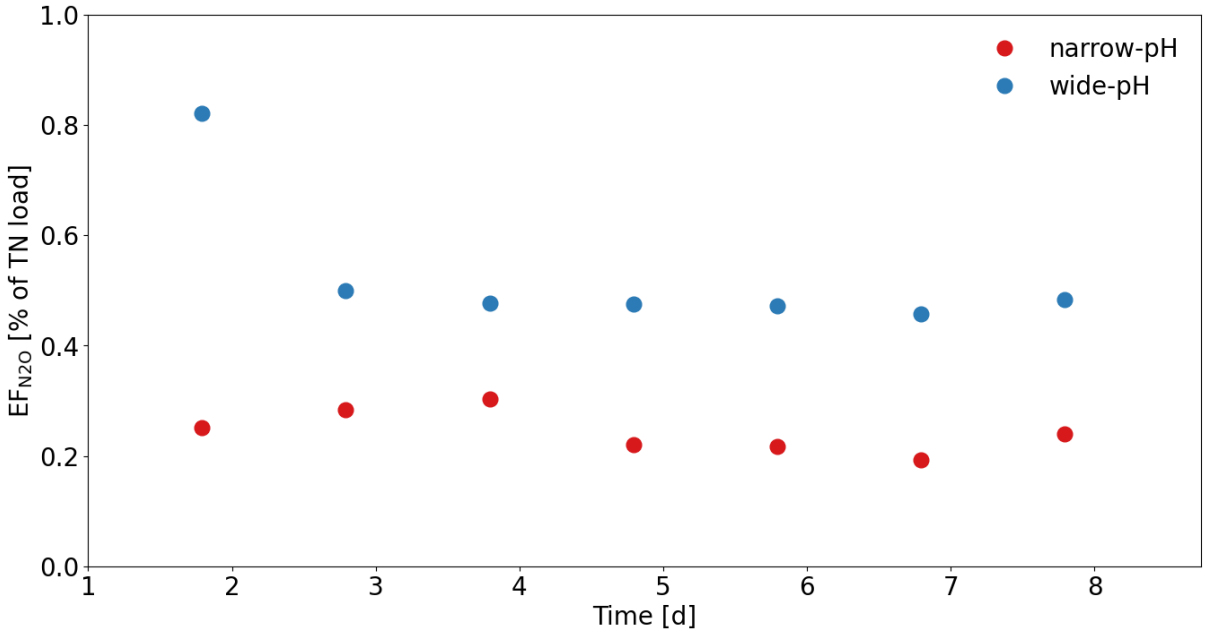

Figure S9: Daily emission factor (EF) of N_2O in the narrow and wide-pH reactor.

8 Alpha diversity of AOB

The alpha diversity of AOB in terms of Shannon and Simpson indices was higher for the wide-pH reactor than for the narrow-pH reactor (**Figure S10**). The mean Shannon indices, not including the first sample, were 0.11 and 0.57 for the narrow and the wide-pH reactor, respectively. The mean Simpson indices, not including the first sample, were 0.04 and 0.25 for the narrow and the wide-pH reactor, respectively.

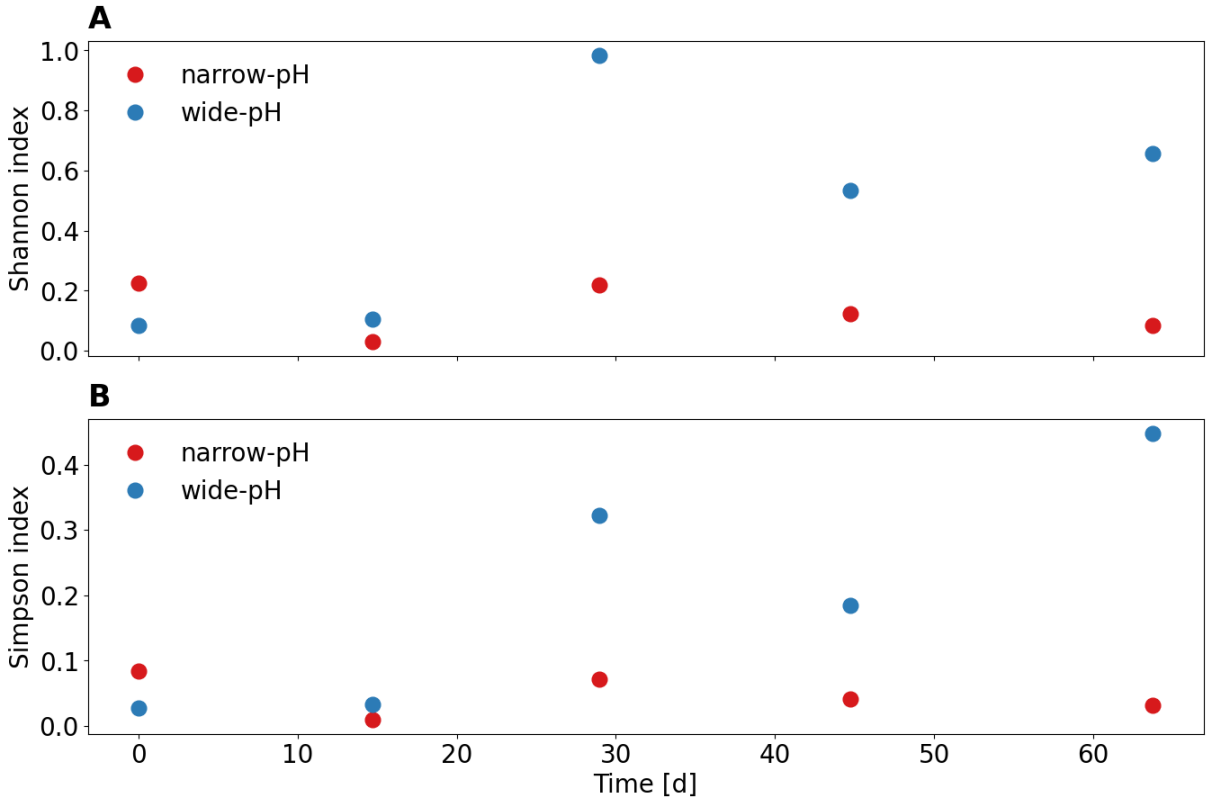

Figure S10: Alpha diversity indices of AOB according to (A) Shannon index and (B) Simpson index of the narrow- and the wide-pH reactor.

9 Phylogenetic tree of major AOB

According to the phylogenetic tree, OUT 15 strongly clustered with *Nitrosomonas europaea* and OUT 59 with *Nitrosomonas halophila* (**Figure S11**).

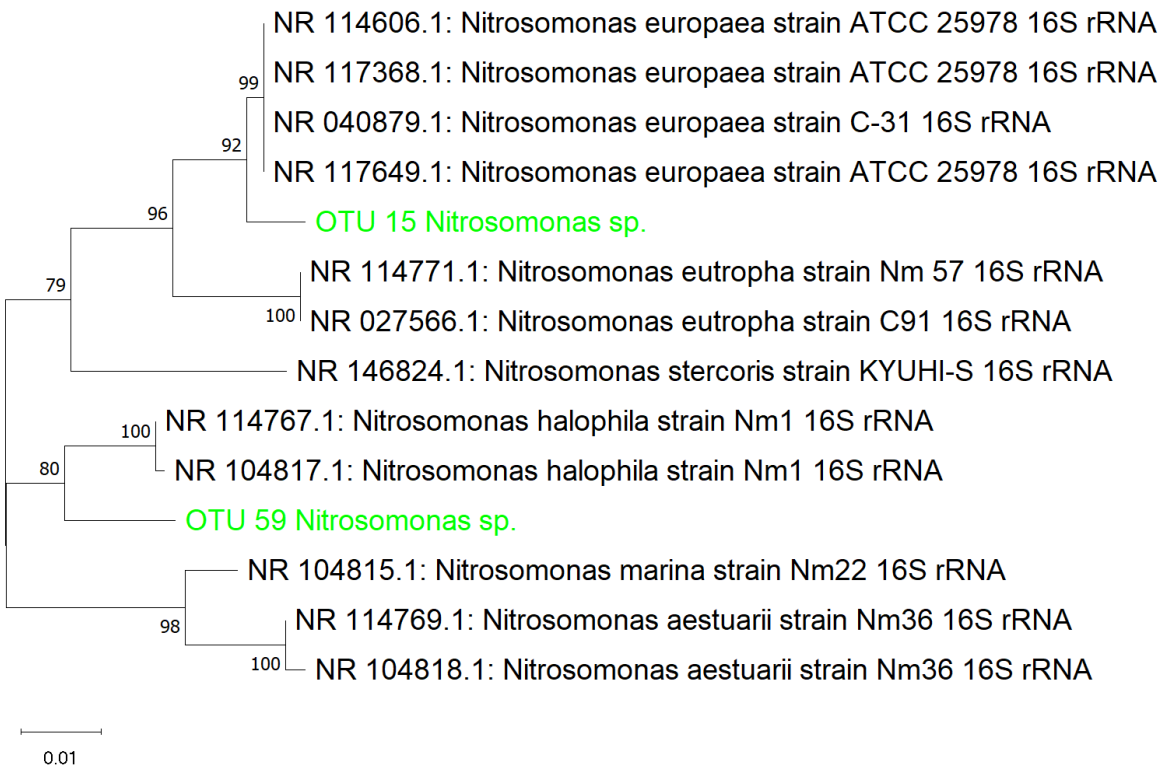

Figure S11: Phylogenetic tree of OTU 15 *Nitrosomonas* sp., which clustered with the *Nitrosomonas europaea* lineage, and OTU 59 *Nitrosomonas* sp., which clustered with the *Nitrosomonas halophila* lineage.

10 Phylogenetic tree of unclassified *Xanthobacteraceae* spp.

Phylogenetic tree of the most abundant unclassified *Xanthobacteraceae* spp. in the biomass sample according to 16S rRNA gene-based amplicon sequencing (**Figure S12**).

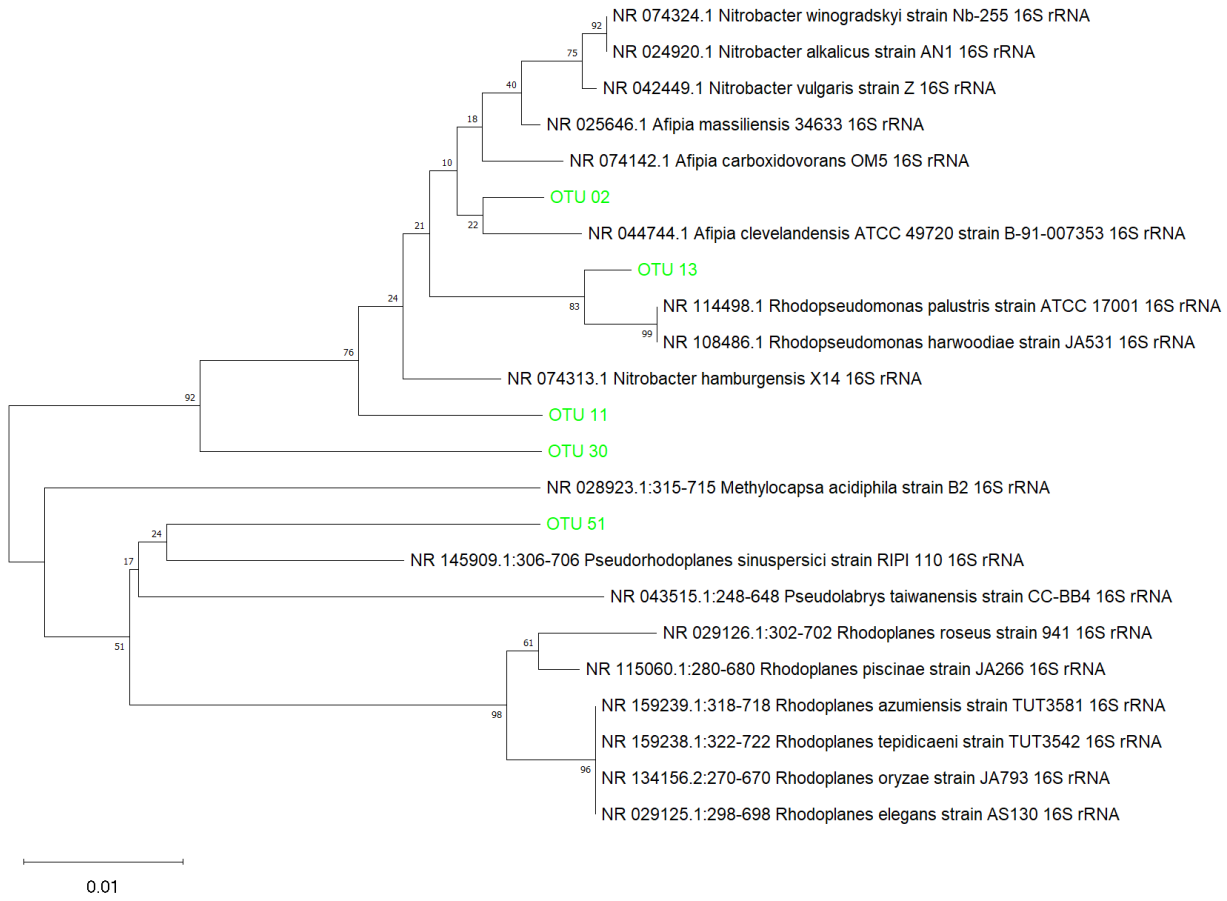

Figure S12: Phylogenetic tree of unclassified *Xanthobacteraceae* spp.

11 Alpha diversity of *Xanthobacteraceae* spp.

The alpha diversity of AOB in terms of Shannon and Simpson indices was higher for the wide-pH reactor than for the narrow-pH reactor (**Figure S13**). The mean Shannon indices, not including the first sample, were 1.7 and 2.1 for the narrow and the wide-pH reactor, respectively. The mean Simpson indices, not including the first sample, were 0.66 and 0.7 for the narrow- and the wide-pH reactor, respectively.

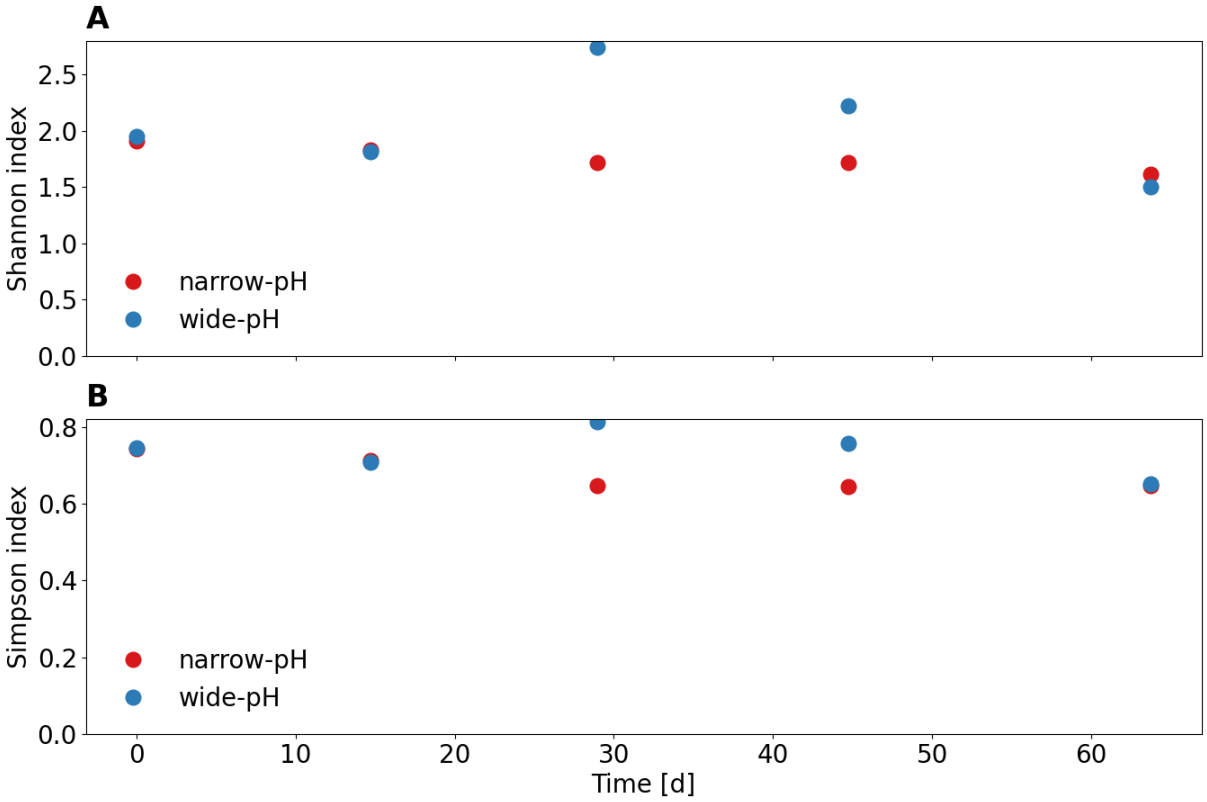

Figure S13: Alpha diversity indices of *Xanthobacteraceae* spp. according to (A) Shannon index and (B) Simpson index of the narrow- and the wide-pH reactor.

12 Alpha diversity of the microbial community

The Shannon and Simpson diversity indices were similar for both operating strategies (**Figure S14**). For both indices, a higher value means a higher diversity.

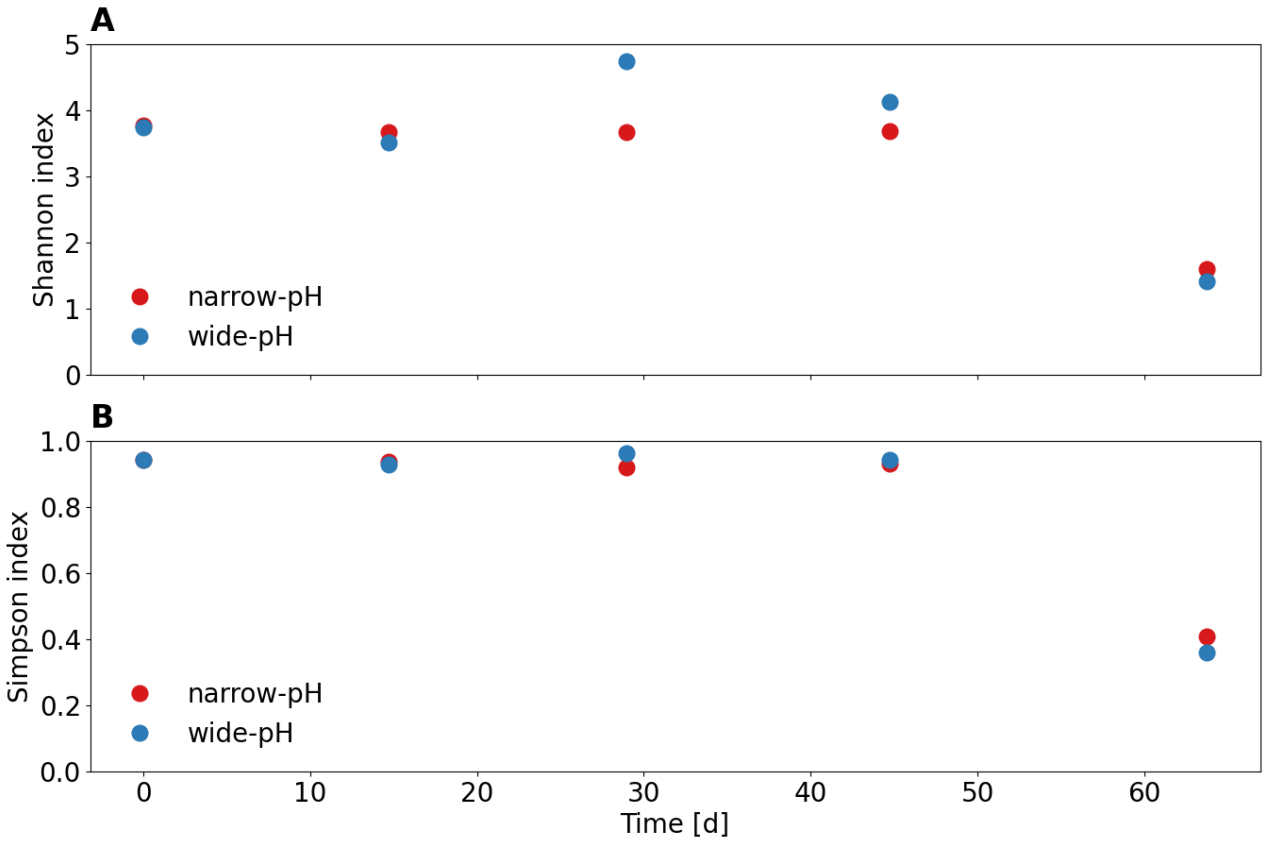

Figure S14: Alpha diversity indices according to (A) Shannon index and (B) Simpson index of the narrow- and the wide-pH reactor.

13 References

ANTHONISEN, A. C., LOEHR, R. C., PRAKASAM, T. B. S. & SRINATH, E. G. 1976. Inhibition of Nitrification by Ammonia and Nitrous-Acid. *Journal Water Pollution Control Federation,* 48**,** 835-852.

CRITTENDEN, J. C., TRUSSELL, R. R., HAND, D. W., KERRY, J. H. & TCHOBANOGLOUS, G. 2012. *MWH's Water Treatment: Principles and Design,* New Jersey, USA, John Wiley & Sons.

DAVIES, C. W. 1967. *Electrochemistry,* London, Philosophical Library.

FAUST, V., VLAEMINCK, S. E., GANIGUÉ, R. & UDERT, K. M. 2023. Influence of pH on urine nitrification: Community shifts of ammonia-oxidizing bacteria and inhibition of nitrite-oxidizing bacteria submitted.

JUBANY, I., CARRERA, J., LAFUENTE, J. & BAEZA, J. A. 2008. Start-up of a nitrification system with automatic control to treat highly concentrated ammonium wastewater: Experimental results and modeling. *Chemical Engineering Journal,* 144**,** 407-419.

LEVINE, I. N. 1988. *Physical Chemistry,* New York, McGraw-Hill.

LEWIS, G. N. & RANDALL, M. 1921. The activity coefficient of strong electrolytes. *Journal of the American Chemical Society,* 43**,** 1112-1154.

STUMM, W. & MORGAN, J. J. 1996. *Aquatic Chemistry: Chemical Equilibria and Rates in Natural Waters,* Wiley.